Article

On Ripples—A Boundary Layer-Theoretical Definition

Ulrich Zanke [1,2,*] and Aron Roland [3]

[1] Z & P—Prof. Zanke and Partner, Ackerstr. 21, D-30826 Garbsen, Hannover, Germany
[2] TU Darmstadt, D-64289 Darmstadt, Germany
[3] BGS-ITE, Pfungstaedter Straße 20, D-64297 Darmstadt, Germany; a.roland@bgsite.de
* Correspondence: zanke@aol.com

Abstract: Once the first initial ripples have developed, they form according to the actual flow forces and sediment properties. In this paper, a semianalytical approach to determine the length of the developed ripples is presented. The theory assumes initial disturbances at the bed surface and corresponding flow separations resulting from an individual respective boundary layer. What causes the initial rhythmic perturbations is not the subject of this paper. Based on boundary layer theory, this approach explains a possible physical background for the existence and length of developed ripples in cohesion-free sediments. At the same time, the approach provides a distinction from dunes: ripples are sand waves affected by a viscous sublayer, and dunes are sand waves where this is not the case. Applications to Earth, Mars, and Titan are shown.

Keywords: sediment transport; ripples; dunes; bed forms; Mars; Titan

1. Introduction

During the transport of granular sediment, a wavy bed forms under certain combinations of flow and sediment, independent of material and nature of the fluid. On the windward side, these bed forms have a slowly rising bed. At a certain position, the accretion of sediment ends and a trough develops. Here, the flow stalls and a roller with horizontal axis is formed (Figure 1). Beginning from the reattachment point, a new boundary layer develops (e.g., Plate 1966 [1]). These sedimentary waves appear in two main forms, the ripples and the dunes. The most striking difference is that ripples are small and in the subaqueous case, if the water depth is greater than about three ripple heights, they are independent of the water depth. According to phenomenological surveys, ripple lengths on earth are $L <\approx 0.6$ m (e.g., Yalin 1964 [2], Allen 1968 [3], Kennedy 1969 [4], Fredsoe 1982 [5], Ashley 1990 [6]). Dunes, on the other hand, are dependent on water depth, both in terms of length and height.

The subject of this paper is the distinction between ripples and dunes in cohesion-free sediments and a theory of their evolved dimensions after they have emerged. For this purpose, a semianalytical approach based on boundary layer theory is developed.
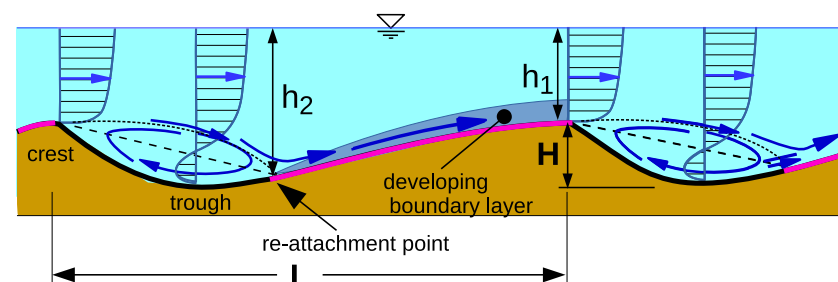
Figure 1. Definitions of dimensions and and characteristic parts of ripples with highlighted developing boundary layer (H = ripple height, L = ripple length, h_1 = water depth at reattachment point, h_2 = water depth at the crest).

2. A Brief Description of the State of Research on the Distinction of Ripples and Dunes

Over decades, based on observations, various diagrams have been developed on the demarcation of the areas of ripples and dunes respectively. Some of these diagrams are dimensional and apply to typical conditions on earth, i.e., sand and water. Examples are criteria in $v - d$ coordinates $v = f(d)$ e.g., Zanke 1976 [7], Southard & Boguchwal 1990 [8] with v = average velocity and d = sediment grain diameter and the associated type of bedform. Other diagrams are dimensionless and therefore more generally. Basis of the dimensionless representations are the dimensionless quantities

$$Re^\star = \frac{v^\star d}{\nu} \tag{1}$$

$$\tau^\star = \frac{v^{\star 2}}{\rho' g d} \tag{2}$$

and their combination

$$D^{\star 3} = \frac{Re^{\star 2}}{\tau^\star} \tag{3}$$

where $v^\star$ = shear velocity, ν = fluid viscosity, $\rho' = (\rho_s - \rho)/\rho$ = relative density, ρ = fluid density and ρ_s = sediment density. Obviously, ripples and dunes can be graphically represented as a function of all these three variables by two-dimensional expressions. The respective third variable is sometimes added as a parameter:

$\tau^\star = f(Re^\star)$ e.g., Chabert & Chauvin 1963 [9].

$D^\star = f(Re^\star)$ e.g., Bonnefille & Pernecker 1966 [10], Vollmers & Giese 1970 [11], Wieprecht 2001 [12].

$\tau^\star \& = \& f(D^\star)$ e.g., v.d. Berg & v.Gelder [13].

This way, the graphical results of the according graphs look quite different although they express widely the same. Burr et al., 2013 [14] showed that the results of bed shape stability (i.e., discrimination of ripple and dune areas) from Southard and Boguchwal 1990 and v.d. Berg and v.Gelder 1993 [13] express almost the same. A similar result was presented by Kleinhans 2005 [15]. Transferring the results of Southard and Boguchwal 1990 [8] to water depths around $h \approx 1$ m as in the Zanke 1976 [7] graph and considering that in Figure 2, d_m is used instead of d_{50}, the blue curve in Figure 2 results. From the above, it is clear that there is widely agreement regarding the demarcation between ripples and dunes. However, the question of "why" is open.
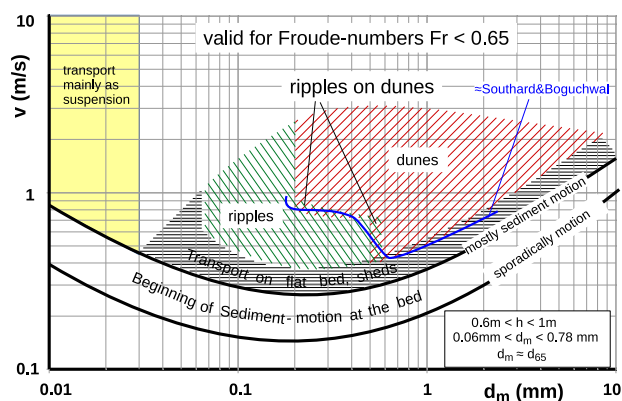
Figure 2. Bed forms as expression of the sedimentological and hydraulic parameters for the sand-water system, modified after Zanke (1976) [7]. For comparison, the limiting curve of the areas of the ripples and the dunes of Southard and Boguchwal 1990 [8] is shown in blue color.

Yalin 1985 [16], based on an evaluation of data from different researchers investigated the length of developed ripples and derived a dimensionless representation which applies to various combinations of liquid and sediment. The result is shown with Figure 3. As long as approximately $X \approx < 3$ results $Y = 1/X$ or

$$\frac{L}{d} \sim \frac{1}{Re^\star} \qquad or \qquad L^\star = \frac{L \, d}{\nu} = const. \tag{4}$$
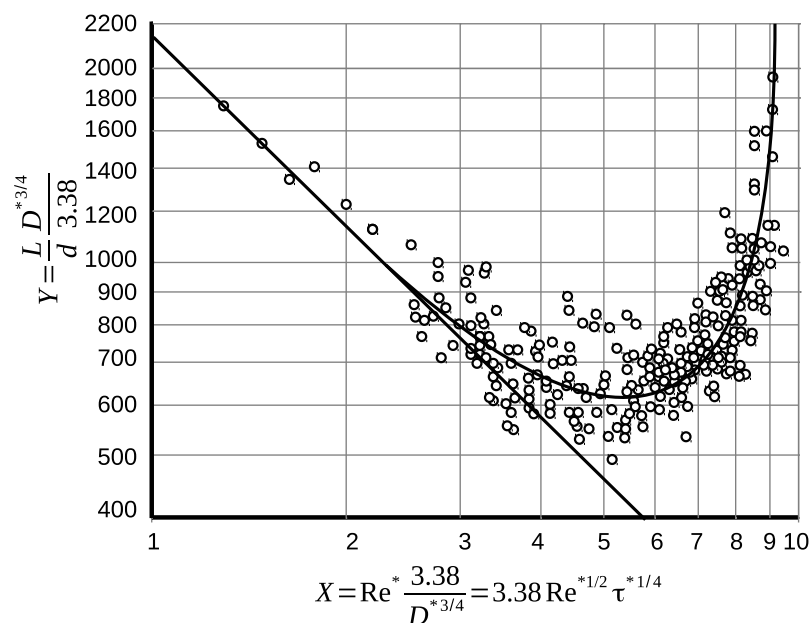
Figure 3. Prediction for ripple lengths according to Yalin [16] based on measurement results of different authors.

As soon as the values at the abscissa rise above about 3, another, still unknown, effect occurs. As a consequence, the ripple lengths deviate from the previously valid trend and increase exponentially.

The most recent data analysis on the delineation of ripples and dunes and on ripple lengths was presented by Lapotre, Lamb and McElroy 2017 [17]. Figure 4 shows their division into ripples and dunes as a function of

$$\chi = Re^\star \sqrt{\tau^\star} = Re^{\star 2} D^{\star -3/2}. \tag{5}$$

The parameter χ is introduced by Lapotre et al. as "Yalin Number". It corresponds to the parameter originally introduced by Yalin in 1985 with Figure 3 where $X = 3.38 \sqrt{Re_d^\star \sqrt{\tau^\star}} = Re^\star D^{\star -3/4}$. Therefore,

$$\chi = \left(\frac{X}{3.38}\right)^2. \tag{6}$$

For comparison purposes, the graphic averaging curve of Yalin's Figure 3 is included in Figure 4 as a red line. It can be seen that the dimensionless ripple length, $L^\star$, strongly increases when $\chi > 4$. Before this background, Lapotre et al. defined a transitional stage between ripples and dunes (in light blue on the figure). By adjusting to the data, Lapotre et al. developed an empirical function for the ripple lengths:

$$L^\star = \frac{v^\star L}{\nu} = 2504 \chi^{1/3}. \tag{7}$$
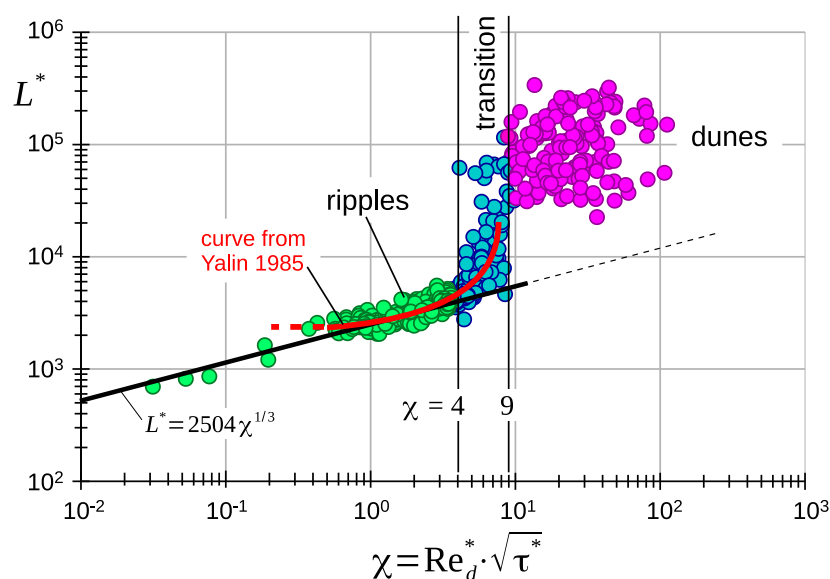
Figure 4. Bed forms and ripple lengths as result of a data evaluation after Lapotre et al., 2017. Green: ripples, magenta: dunes, blue addressed as an intermediate stage. The red line shows the mean course of the data from Yalin 1985 (Figure 3).

3. Data Used for Comparison Purposes

For comparison with measured ripple dimensions, in this paper the same data set was used as that for the investigations by Lapotre et al., 2017 (Figure 4). These 473 data (from Barton and Lin [18], Vanoni and Brooks [19], Stein [20], Guy et al. [21], Williams [22], Alexander [23], Bishop [24], Mantz [25], Grazer [26], Gabel [27], Baas [28], Venditti et al. [29]) were provided by M. Lapotre and were supplemented here with further 39 data sets from Kühlborn 1993 [30].

4. Semi Analytical Approach to Length and Domain of Ripples

4.1. Theory

As soon as initial ripples have formed, they start to grow. However, this growth is limited, as the observation shows. Yalin 1985 [16] represents the fully developed ripple length by a dimensionless diagram (Figure 3) and defines ripples up to $X \approx 9 \ldots 10$. In contrast, Lapotre et al., 2017 interpret the sand waves in the $4 < \chi < 9$ range as a transition between ripples and dunes. The position of $\chi = 4$ in Figure 4 corresponds to $X \approx 6.7$ in Figure 3. A discrepancy is obviously in the range of $\chi < 1$, as the Yalin curve in the Lapotre diagram of Figure 4 shows.

In the following it is shown how the formation of ripples can be described with instabilities of the viscous boundary layer as principally shown in Figure 5 for a developing boundary layer at a plane plate. Behind each embryonic ripple crest a new boundary layer starts and develops like that demonstrated in the figure. This boundary layer is initially laminar, i.e., viscous. Sooner or later, depending on the roughness of the bed, the flow velocity and the degree of disturbance of the outer flow, it switches to a turbulent boundary layer.

As the shear stress along a developing viscous boundary layer over a flat bed decreases along the path, sediment is retained and forms a rising bed. Sediment accumulation only ends when the shear stress along the path at each position is sufficient to transport the incoming sediment load further. This is shown schematically in Figure 6. The simultaneous growth of a windward slope (=stoss side) breaks off as soon as the boundary layer turns into a turbulent boundary layer. In Figure 6 this is illustrated too. The initially viscous sublayer switches into a turbulent boundary layer when a critical Reynolds number is exceeded. At that position, a sudden increase of bed shear stress occurs. As a consequence of this abrupt increase in shear stress, the sediment transport rate also increases abruptly.

This transport imbalance leads to local erosion, which results in a ripple trough and this way determines the ripple length. The sediment transport on the stoss side is strongly influenced by sweeps and burst from the outer flow. The possible effect of this is not investigated here.
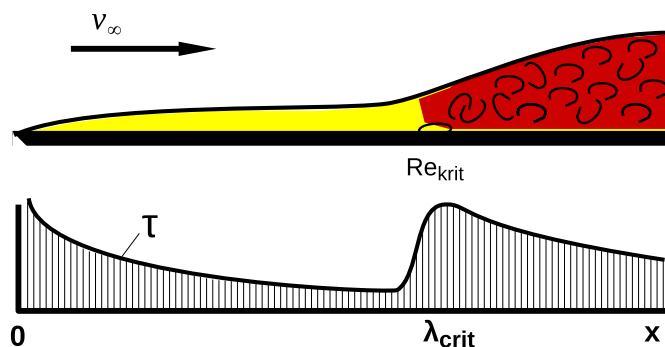
Figure 5. Development of the boundary layer along a flat plate with laminar-turbulent changeover (**top**) and local shear stress on the plate (**bottom**).
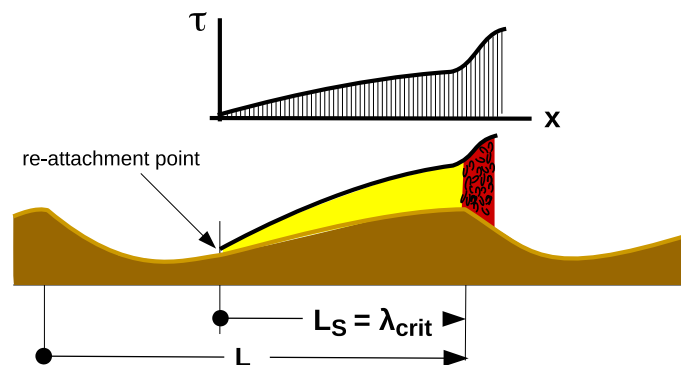
Figure 6. Principle sketch of the development of a ripple starting from initial disturbances on a flat bed. The stoss-side develops from a flat bed in a feedback process with the boundary layer. Sediment is retained and, at the same time, the local shear stress increases until transport is balanced at each location.

According to the relevant literature (e.g., Schlichting 1965 [31], Schlichting and Gersten 2005 [32]) the relatively sudden switch from laminar to turbulent boundary layer occurs at a Reynolds number formed with the running length from the beginning of the boundary layer, $x = \lambda_{crit}$:

$$Re_{crit} = \frac{v_\infty \lambda_{crit}}{\nu} = a_u \tag{8}$$

with $a_u \approx 3 \times 10^5 \ldots 10^6$. The value of a_u clearly depends on the degree of turbulence of the outer flow velocity, v_∞. In case of strong external turbulence, a_u is smaller than 3×10^5 but can be much larger in case of a very low degree of disturbance of the external flow [31,32]. In the present case, the turbulence is particularly increased at the beginning of the developing boundary layer, i.e., at the reattachment point. With the local resistance coefficient of the viscous boundary layer [31,32]

$$c_f = 0.664 \left(\frac{v_\infty x}{\nu} \right)^{-\frac{1}{2}}. \tag{9}$$

With also $c_f = 2 \left(\frac{v^\star}{v_\infty} \right)^2$, at the position $x = \lambda_{crit}$ yields

$$c_f = 2 \left(\frac{v^\star}{v_\infty} \right)^2 = 0.664 \left(\frac{v_\infty \lambda_{crit}}{\nu} \right)^{-\frac{1}{2}}. \tag{10}$$

This can be transformed into

$$\frac{v^\star \lambda_{crit}}{\nu} = 0.577 \, a_u^{3/4}. \tag{11}$$

An adaptation to available 512 ripple data results in

$$a_u = 7.82 \times 10^4 \tag{12}$$

This value is lower than the values obtained from wind tunnel tests of about $a_u = 3 \times 10^5$. However, there is consensus that the external turbulence has a considerable influence on the turn over to a turbulent boundary layer [31,32]. In the boundary layer along the windward slope of the ripple, this is the case to a considerable extent. The corresponding critical value of

$$\frac{v^\star \lambda_{crit}}{\nu} = 2700. \tag{13}$$

is therefore quite realistic. The distance λ_{crit} corresponds to the length of the windward slope, L_S. With Figure 7 can be approximated

$$(L - L_S) \, \tan \alpha = L_S \, \tan \beta \tag{14}$$

or

$$\frac{L_S}{L} = \frac{1}{\frac{\tan \beta}{\tan \alpha} + 1} \tag{15}$$

and

$$\tan \beta = \frac{1}{\frac{L}{H} - \tan \varphi}. \tag{16}$$
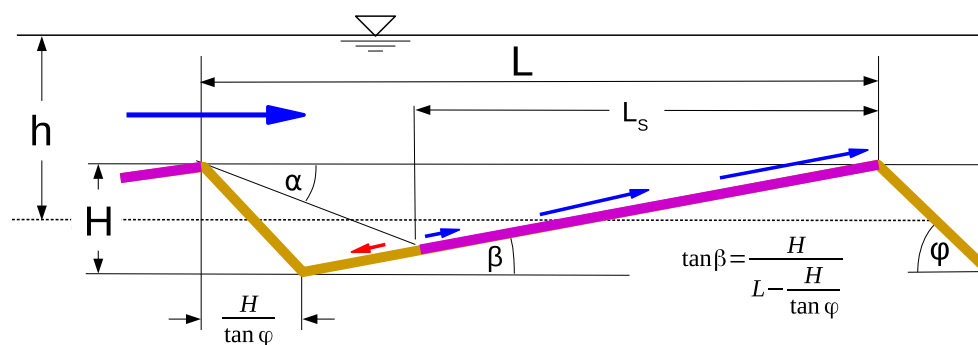
Figure 7. Definitions of the parameters used here to describe the ripple geometry.

Recent in-depth investigations of the flow over two-dimensional sand waves have been carried out by Dey et al., 2020a [33], Dey et al., 2020b [34] based on experiments and by Zhao 2021 [35] based on numerical modelling. These investigations largely agree with respect to the angle α and confirm earlier investigations (e.g., Schlichting [31]) at an angle of about 9° to 10°. For a mean slope of $H/L = 1/11$, an angle of repose of $\varphi = 30°$, and a separation angle of $\alpha = 9^o$, the windward slope $\lambda_{crit} = L_S \approx 0.6\,L$. This ratio is not very sensitive to a variation of the angles in the natural environment. Thus one obtains for the ripple length

$$L^\star = \frac{v^\star L}{\nu} \approx \frac{0.577}{0.6} \, a_u^{3/4} = 4500. \tag{17}$$

and in a different notation

$$\frac{L}{d} = \frac{L^\star}{Re^\star} \approx \frac{4500}{Re^\star} = \frac{4500 \, \sqrt{\tau^\star}}{\chi}. \tag{18}$$

According to Equation (18) all measurement results for the dimensionless ripple lengths would have to coincide on the level $L^\star = 4500$ or $\frac{L}{d} = \frac{4500}{Re^\star}$. These are the light blue arithmetic crosses in Figure 8. Although the general trend of measured $L/d \sim 1/Re^\star$ agrees with the theory, there is a shift for the mass of the data and a deviating trend for the data marked by the red ellipse. The reason for this is obviously an effect that overlays the boundary layer effect. This is discussed in the following.

4.2. Consideration of the Effect of Sediment Suspension

Starting with very small $Re^\star$ numbers, the ripples become shorter with increasing $Re^\star$ numbers for a given grain size, as long as $X < 3\ldots4$ (Figure 3). In this respect, the theory worked out so far (Equation (18)) agrees with the measured trend as long as about $\chi < 3\ldots4$. However, there is a parallel shift between the green measured data and the light blue arithmetic crosses in Figure 8.

Furthermore, some deviations from the trend in Equation (18) are particularly evident in the values marked by the red ellipse. The respective data are from Grazer 1982 [26]. While most of the measured data concern sand, driven by water at the temperature range of $10° < T < 20°$, the extreme data from Grazer are characterized by particularly very fine and light sediment driven by sucrose-water mixtures. The particle Reynolds numbers are here in the range of $0.03 < Re^\star < 0.33$ and the ratio between shear velocity and settling velocity, $v^\star/w$, which is characteristic of the suspension, is 10 to 100 times the other measured data. The data point on the far left for example is marked by $d = 0.02$ mm, $\rho' = 1.17, \nu = 1.05\,10^{-5}\,\text{m}^2/\text{s}, Re^\star = 0.03$, i.e., very fine sediment and a thick liquid. Grazer reports that the ripples are caused by bed load transport, which, however, accounts for less than 5% of the total load in his experiments. The ratio of $v^\star/w$ (the reciprocal of the Rouse number), which describes the degree of suspension, is up to $v^\star/w = 620$ in these data.

Different effects are connected with high suspension over ripples. Already in 1940 Vanoni [36] stated that the velocity profiles are changed by high concentrations of suspended matter near the bed. He attributed this to a damping of the turbulent velocity fluctuations. Vanoni explicitly states: "Suspended sediment in a flow tends to reduce appreciably the turbulent transfer of momentum and hence the resistance to flow, allowing the sediment-laden water to flow more rapidly than a comparable clear water flow. This effect increases with the total sediment load and with a decrease in the grain size of the sediment". In addition, various later studies (e.g., Toorman et al. [37] and others) describe a reduction in wall friction with simultaneous thickening of the viscous boundary layer as an effect of an increased concentration of suspended matter near the bed. However, in case of ripples, these effects, namely reduction of shear stress and thickening of the viscous boundary layer, are superimposed by another effect:

In the case of pure bed load, sediments eroded along the windward slope are completely deposited on the leeward slope. This is absolutely necessary for a migration of the ripples without volume loss. However, this is only partially the case with sediments that move in suspension. The more sediments are transported in suspension, the smaller the proportion that is deposited on the lee side and thus contributes to the preservation of the ripple length. Consequently, high values of v/w and thus also of $v^\star/w$ lead to a shortening of the ripples up to their complete washing out.

Empirically, with adaptation to the available ripple data, the suspension effect can be described by

$$L^\star = \frac{4500}{S} \tag{19}$$

with

$$S = 1 + (v^\star/w)^{1/4}. \tag{20}$$

Equation (19) can also be expressed by

$$\frac{L}{d} = \frac{4500}{Re^\star \times S} \tag{21}$$

or

$$\frac{L}{d} \times \frac{1}{\sqrt{\tau^\star}} = \frac{4500}{\chi \times S}. \tag{22}$$

The settling velocity needed in Equation (20) can be determined from Zanke 1977 [38]

$$w = \frac{12\,\nu}{d\,(2.7 - SF)} \left(\sqrt{1 + (0.21\,D^\star)^3\,(2.7 - 2.3\,SF)} - 1 \right). \tag{23}$$

where SF is the shape factor after McNown and Malaika 1950 [39]. For sand from natural waters $SF \approx 0.7$ and then

$$w = \frac{11\,\nu}{d} \left(\sqrt{1 + 0.01\,D^{\star 3}} - 1 \right). \tag{24}$$

The effect of S has provided a good approximation and is shown in Figure 8 with the calculated results in magenta color.
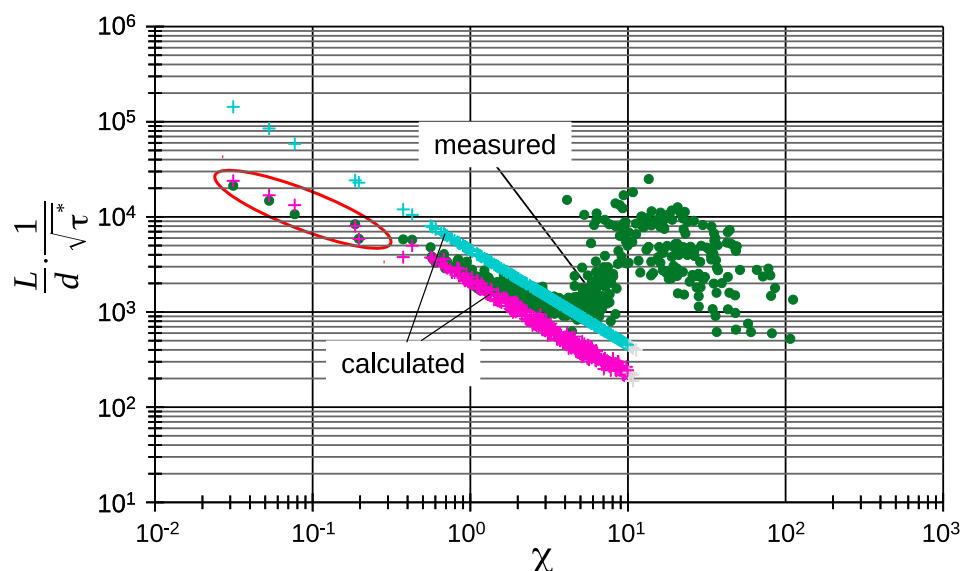
Figure 8. Comparison of the measured data (green), Equation (18) (blue) and Equation (22) (magenta). The difference of the two equations describes the individual effects of suspension (Note: In the range of $\chi > 9$, according to Lapotre et al., 2017, bed forms are dunes.) For data source, see Section 3.

4.3. Consideration of the Effect of Acceleration of the Boundary Layer Flow

4.3.1. Acceleration-Related Maintenance of Viscous Boundary Layer

The Equations (19)–(22) satisfy the measurement data up to Yalin numbers of $\chi \approx 1$. In the direction of larger χ the ripple lengths leave the trend $L/d \sim 1/Re^\star$ and increase, first slowly and from about $\chi = 4$ rapidly. Regarding Nikuradse's commonly known findings on roughness effects, one would expect the end of the ripples to be at $Re^\star > \approx 5$ if they were based on a viscous boundary layer. Obviously, another effect seems to prevent this. This is possible in principle with accelerated flow, and such an effect is actually present on the windward slopes. In accelerated flows the transition to turbulence is delayed. With this respect, research on relaminarization of turbulent flows is of interest. For the case of relaminarization of an accelerated, turbulent boundary layer, the literature specifies as a limiting factor:

$$K = \frac{\nu}{v_\infty^2} \frac{dv_\infty}{dx} > 2 \times 10^{-6} \dots 3.5 \times 10^{-6} \tag{25}$$

(e.g., Launder 1964 [40], Schlichting & Gersten 2005 [32]). K is the critical level up to which the relaminarization of a previously turbulent boundary layer is possible due to an acceleration of the flow. It is v_∞ the flow velocity at the boundary layer edge.

We postulate that K is also decisive with respect to maintaining a viscous boundary layer by retarding the laminar-turbulent transition. In addition, we assume that K also characterizes to a large extent the end of the maintenance of an existing viscous boundary layer. Presumably, maintenance of the existing laminarity is associated with slightly smaller K values than for the suppression of existing turbulence.

In case of ripples, acceleration takes place beginning at the reattachment point up to the crest from $v \approx 0$ to v_∞. Strictly speaking, only the mean velocity at the reattachment point is zero. This may have an influence on the effective value of the acceleration. This question is not investigated here. If we simplify $\frac{dv_\infty}{dx} \approx \frac{\Delta v_\infty}{\Delta x} = \frac{v_\infty}{\lambda_{crit}}$ then ripples can exist as long as

$$\frac{\nu}{v_\infty \lambda_{crit}} > 2 \times 10^{-6} \dots 3 \times 10^{-6} \tag{26}$$

or

$$\frac{v_\infty \lambda_{crit}}{\nu} < 3.3 \times 10^5 \dots 5 \times 10^5. \tag{27}$$

Equation (10) can be converted to

$$\frac{v_\infty}{v^\star} = 3^{2/3} \left(\frac{v^\star \lambda_{crit}}{\nu} \right)^{1/3} \tag{28}$$

with which one yields

$$\frac{v^\star \lambda_{crit}}{\nu} = 0.577 \left(\frac{v_\infty \lambda_{crit}}{\nu} \right)^{3/4}. \tag{29}$$

This results in the criterion for estimating the acceleration-related limit of maintenance of the viscous boundary layer and thus the conditions for the length of the ripples stoss side:

$$\frac{v^\star \lambda_{crit}}{\nu} < 7.9 \times 10^3 \dots 1.1 \times 10^4. \tag{30}$$

After considering $\lambda_{crit} \approx 0.6\,L$ (Figure 7) finally follows for the limit of the existence of ripples

$$\left(\frac{v^\star L}{\nu} \right)_{lim} = L^\star_{lim} \quad < \quad 1.34 \times 10^4 \dots 1.83 \times 10^4. \tag{31}$$

As mentioned above, the critical value up to which laminarity can be maintained is most likely somewhat higher in the case of avoiding turbulence than in the case of completely damping existing turbulence. It is important to note that the laminar reference Equation (10) is valid for flat plate boundary layers without acceleration. Nevertheless, it proves to be representative here as Pschernig 2017 [41] lined out, based on measurements. The c_f values measured by Pschernig after relaminarization were somewhat higher than those after Equation (10), so that the calculated values of Equation (31) could well be determined somewhat higher.

Based on a comparison with the measured data, we assume that the limit of ripple existence is phenomenologically well described due to the discontinuity in the wave lengths at the blue-magenta boundary in Figures 9 and 10 by

$$L^\star_{lim} \approx 30,000 \quad \text{or} \quad \left(\frac{L}{d} \right)_{lim} \approx \frac{30,000}{Re^\star} \quad \text{or} \quad \left(\frac{L}{d \sqrt{\tau^\star}} \right)_{lim} \approx \frac{30,000}{\chi} \tag{32}$$

Figure 9 shows the latest at $\chi \, > \approx 4$; the effect of acceleration dominates and ends at $\chi \, > \approx 8 \dots 9$ (blue data points). This can explain the transition range defined by Lapotre et al. (Figure 4).

4.3.2. Solution Proposal for the Calculation of the Effect of Boundary Layer Acceleration

From the comparison with the measured values an approximate empirical function for the acceleration-related value of a_u in Equation (8), results:

$$A = \left(\frac{a_{u,acc}}{a_u}\right)^{3/4} = \frac{1}{(1 - \chi/9)^{1.35}} \tag{33}$$

Here A is the acceleration-related factor in respect to $L^\star$. With Equations (19) and (33) results

$$L^\star = 4500 \times \frac{A}{S}. \tag{34}$$

and the same physics in a different notation reads

$$\frac{L}{d} = \frac{4500}{Re^\star}\frac{A}{S} \quad \text{or} \quad \frac{L}{d\sqrt{\tau^\star}} = \frac{4500}{\chi}\frac{A}{S} \tag{35}$$

which is shown in Figures 9 and 10 with the red symbols as "calculated" results.
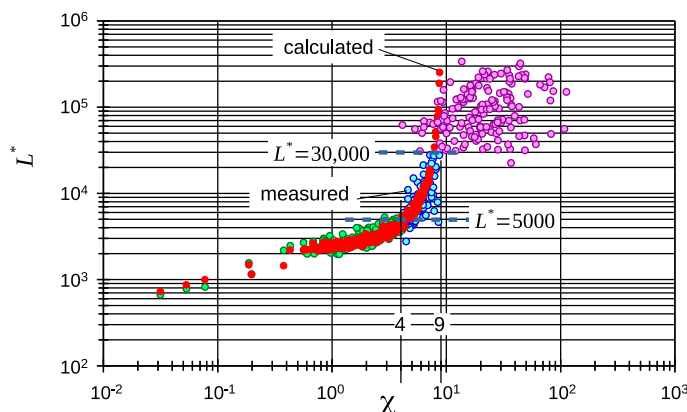
Figure 9. Comparison of the measured data and Equation (34) (red). For data source, see Section 3.
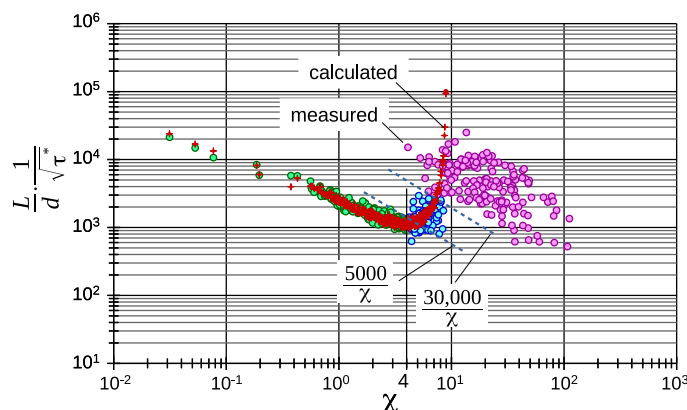
Figure 10. Comparison of the measured data and Equation (35) (red). For data source, see Section 3.

5. Reflections on the Limits of the Ripple Domain

5.1. Upper Limit

Literature: With regard to the interconnections in Equation (3) it is understandable that ripple criteria have also been developed on the basis of $Re^\star$ as well as on the basis of $D^\star$. e.g., Chabert and Chauvin 1963 [9], Bonnefille and Pernecker 1966 [10], Vollmers and Giese 1970 [11], and Wieprecht 2001 [12] describe the upper boundary of the ripple domain by a critical Reynolds number with a variation of about $10 < Re^\star < 20$. For example, Wieprecht mentions $7 < D^\star < 18$, while after v.d. Berg and v.Gelder about $3 < D^\star < 18$ is

appropriate. Duran 2019 [42], based on evaluations of the results of a numerical channel with coupled hydromechanics and sediment transport, estimated $Re^\star \approx 20 \ldots 25$ as a limit.

This paper: With the theory presented, due to the effects of flow acceleration at the windward slopes of the ripples, these are limited with $L^\star \approx 30{,}000$. It is worth mentioning that in the numerical channel of Duran et al. the upper limit of the ripple range is at $L^\star \approx \ldots 15{,}000 \ldots 20{,}000$. The data recorded by these authors show ripples up to about $L^\star \approx 25{,}000$. This confirms the order of $L^\star$ resulting from our theoretical approach.

From Figures 9 and 10 it can be seen that this fairly corresponds well to $\chi \approx 9$, which thus provides an explanation for the limit established by Lapotre et al., 2017. With the definition of χ from Equation (5) and $\chi = 9$, the following results for limiting $Re^\star$ and $D^\star$ are

$$Re^\star = \frac{9}{\sqrt{\tau^\star}} \qquad and \qquad D^\star = \left(\frac{9}{\tau^\star}\right)^{2/3}. \tag{36}$$

Thus ripples exist in the range of e.g., $0.05 < \tau\star < 1$ at about $40 > Re^\star > 9$ and $30 > D^\star* > 4.3$. Based on $\chi = 8$ as a boundary results $36 > Re^\star > 8$ and $29 > D^\star* > 4$. Figure 11 shows an evaluation of the $Re^\star$ numbers in the case of ripples from an excerpt of the data set. The effect of boundary layer acceleration proposed in this paper can explain the existence of ripples up to Reynolds numbers in the range of 30 or even 40. Such values occur when the Yalin number $\chi \to 9$, while the shear stress is only slightly above the critical value. This result is in good agreement with the data analyses of Lapotre et al., 2017 (their Figure 2C). At the same time, $L^\star \approx 30{,}000$.

Based on the considerations about the effect of flow acceleration on windward slopes, it can also be understood why the ripple formation, although dominated by the viscous boundary layer, does not end at $Re^\star \approx 5$, as would be expected according to Nikuradse.
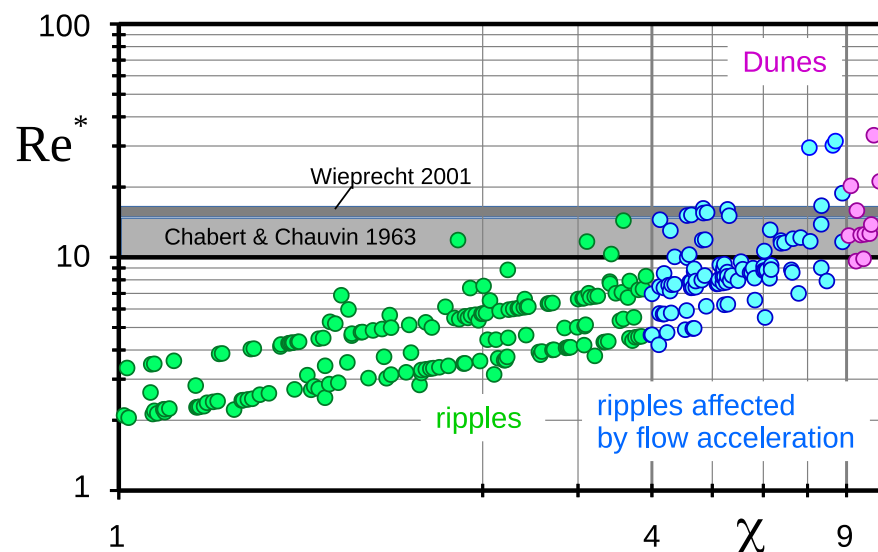
Figure 11. $Re^\star$ at the upper limit of the ripple domain from the data set used and from two data-based diagrams from the literature (Chabert and Chauvin 1963 and Wieprecht 2001) as an example. For data source, see Section 3.

5.2. On the Lower Limit Particle Size of Ripple Existence

The question of a lower limit of ripple existence, related to grain size, e.g., arises when comparing different representations of the range of ripples. For example, according to Figure 2 (Zanke 1976), ripples do not occur in the silt-water system. On the other hand, the investigations of e.g., Grazer 1982 [26] show ripples even at $d \approx 0.02$ mm.

Zanke's observations (Figure 2) are based on a natural sediment from the area where the freshwater of the Eider in Northern Germany flows into the salty North Sea. As a result of the brackish water, silt with a cohesive effect on the fine sands is generated. Therefore,

depending on the grain size and the amount of cohesive parts, these sediments do not develop ripples.

The experiments of Grazer, however, are explicitly based on noncohesive sediments. From this it can be concluded that cohesion can limit the existence of ripples in fine sediments.

5.3. The Transition Range

Lapotre et al., 2017 defined a transition between ripples and dunes with $4 < \chi < 9$ (Figure 4). Here we come to the conclusion that this range is dominated by the effect of flow acceleration on the turnover from viscous to turbulent boundary layer. This means that the bed forms in this range are ripples which are characterized by the acceleration effects of the viscous boundary layer. At $\chi \approx 4$ in our view of the problem there is no real limit but the change in the dominance of two different effects.

In contrast, there is a real limit of the ripple domain at $L^\star \approx 30{,}000$, which corresponds quite well with $\chi = 9$ and thus confirms each other. This can be drawn from Figure 12.
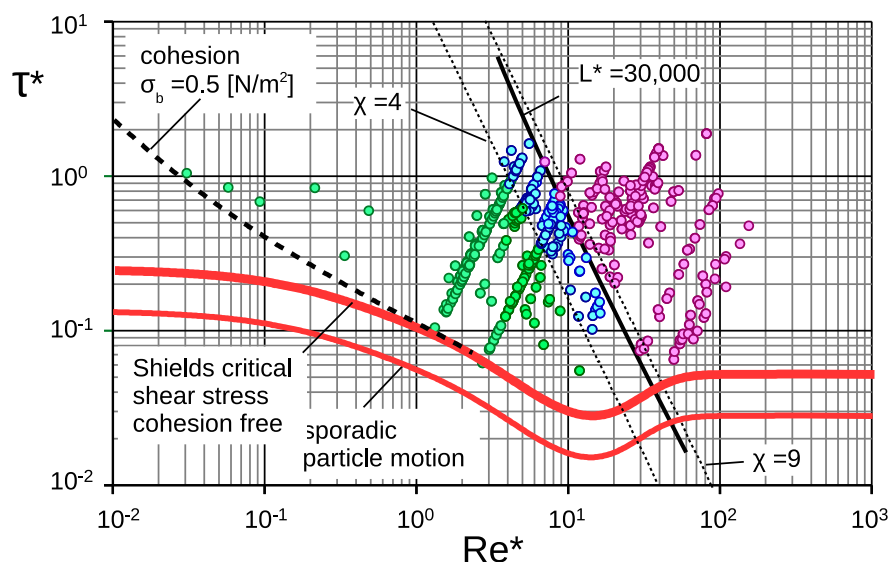
Figure 12. Representation of the domain boundaries in the $\tau^\star - Re^\star$-plane. Ripples exist in the green and blue areas. In the green area the ripples are dominated by the Reynolds number $v^\star d / \nu$ and are modulated by the degree of suspension concentration. The area marked blue is dominated by the effect of boundary layer acceleration. For data source, see Section 3.

6. An Alternative Presentation of Data only by Boundary Layer Effects

In the previous sections, the data were plotted as measured and the boundary layer theoretical solution was adjusted for the effect of the suspension, Equations (19)–(22). Alternatively, **the measured data can be adjusted for this effect** as in Figures 13 and 14. This means that the original data here are adjusted for the effect (S) caused by the suspension. The ordinate $L^\star S$ thus represents the mathematically adjusted effective value for $L^\star$. Thus, the data take a course as it would be expected without the effect of the suspension. Then, for small values of χ (i.e., with insignificant influence of acceleration), a course is obtained which corresponds to the purely boundary layer theory based Equation (18) (line 184 revised manuscript version). The y-values of the data in these Figures are therefore correspondingly higher as the reduction of ripple length due to suspension is eliminated. This procedure allows the boundary layer effects to be represented in an isolated form.
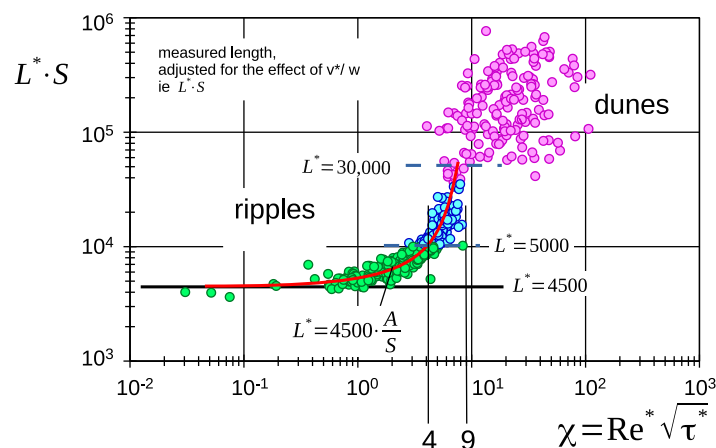
Figure 13. Dimensionless length of ripples and dunes, $L^{\star}$, as well as their subdivision according to boundary layer instabilities. The data are **adjusted for the suspension effect.** The ripples, dominated by the acceleration effect are colored in blue. Red curve: Equation (34). For data source, see Section 2.
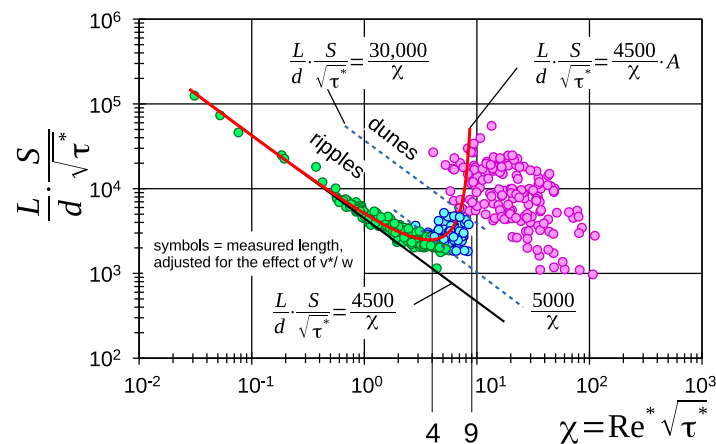
Figure 14. Relative length of ripples and dunes, L/d, as well as their subdivision according to boundary layer instabilities. The data are **adjusted for the suspension effect**. The ripples, dominated by the acceleration effect, are colored in blue. Red curve: Equation (35), Black line: Equation (35) with $A = 1$. For data source, see Section 3.

7. Examples of Ripple Domain and Length on Earth, Mars, and Titan

Ripples can obviously occur wherever fluid flows over granular media. In addition to the Earth, sand waves have been observed for various planets such as Mars or Venus, as well as for the dwarf planet Pluto and Saturn's moon Titan, although liquid and sediment are very different. On Earth, knowledge about ripples and dunes is both a practical and scientific issue, as they affect sediment transport and through their roughness effect have an impact on water levels in the subaqueous case.

Sand detected on Titan consists of granular, frozen ammonium sulfate and the atmosphere is mainly of methane and nitrogen. Some examples of data, relevant for sediment motion, are summarized in Table 1. These are at first the relative density, the gravity, and the fluid viscosity. A special case with a light weight sediment as used in physical hydraulic models with movable bed is added. In the literature, the relevant data of other planets sometimes differ slightly from each other and should be understood as approximate values. On the one hand, this is related to the status of the explorations and on the other hand it is due to different locations and seasons. The data on gravity acceleration also vary slightly. For example, Almeida et al., 2008 [43] name for Mars in case of wind driven

sediment motion $\rho = 0.02$ kg/m^3 and $\rho_s = 3200$ kg/m^3 while after Lapotre et al. 2017 [44] 0.002 kg/m$^3 < \rho < 0.02$ kg/m^3 and $\rho_s = 2900$ kg/m^3.

Figure 15 shows for some examples that the domain of the ripples is on the one hand limited by the beginning of sediment motion and is on the other hand limited by $L^\star \approx 30{,}000$.

According to many observations, the beginning of the ripple formation is slightly above the critical value for the beginning of motion according to Shields 1936 [45]. The point of intersection of these two limits coincides with about $20 < Re^\star < 30$, which also agrees with observations. With exceeding the critical conditions for the beginning of the movement (here $v_c^\star$) comparatively long ripples develop. With increasing $v^\star$, the length decreases and achieves a minimum value at $\chi \approx 4$. Then the lengths increase until the limit of the ripple domain at $L^\star \approx 30{,}000$ is being reached. This coincides approximately with $\chi \approx 9$. For larger grain sizes, the beginning of the movement may coincide with $\chi >= 4$. Then the ripple length does not decrease after exceeding $v_c^\star$ but immediately increases with $v^\star$. Thus the limiting factors are summarized as follows:

1. **Critical shear stress**. Ripples only develop when $\tau >\approx \tau_c$ and $L^\star \approx< 30{,}000$ which coincides with $\chi \approx 9$.
2. **Re* > 20…40**. If the theoretical length would be $L^\star = 30{,}000$, but the actual shear stress is still subcritical, so no ripples can emerge. This happens when $Re^\star > 20\ldots40$ (Figures 12–15).

In many natural waters on Earth the beginning of the ripple development is influenced by cohesive sediment components. In Figures 15 and 16, the black dashed curve in the case of sand-water shows the beginning of sediment movement in natural sand mixtures with cohesive components typical for rivers. This curve is based on the curve developed by Hjulström 1935 [46]. Finally, Figure 17 shows the results of Equation (35) for the ripple length vs. sediment particle diameter, d. As you can see, in case of the earth Equation (35) is in good agreement with the observations with a maximum of $L \approx 0.6\ldots0.8$ m. On Mars and Titan, however, depending on the constellation of ρ', g, ν, d, several meters of length are possible. This is also in accordance with respective observations (e.g., [44]).
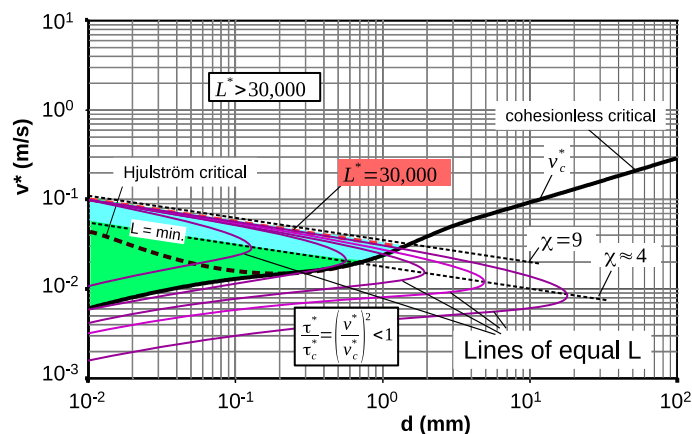
Figure 15. Ripple domain, example for the case Earth-sand-water.

On both Mars and Titan, the subaqueous ripples can become larger than on Earth and can grow to some meters in length. For Titan, Perron et al., 2006 [47] report seasons with significant temperature variability. The viscosity of liquids and "air" therefore varies with the summer and winter seasons. Based on the example data of Table 1 and using Equation (35), the ranges of existence and ripple lengths are calculated and displayed on Figure 16. The figure on the top right shows the calculated ripple characteristic in case of hydraulic models with polystyrene sediment in water.

Table 1. Some characteristic data of planets with respect to ripples.

Planet	g (m/s²)	ρ'	ν (m²/s)
Earth (Sand-Water)	9.81	1.65	1×10^{-6}
Earth (Polystyrene-Water)	9.81	0.03	1×10^{-6}
Mars (liquid fluid) *	3.78	1.04	4×10^{-5}
Titan (liquid fluid) *	1.35	0.85	5×10^{-6}
Earth (Sand-Air)	9.81	2160	1.5×10^{-5}
Mars (Sand-Air) **	3.78	1.45×10^{5}	5.4×10^{-4}
Mars (Sand-Air) ***	3.78	1.45×10^{6}	5.4×10^{-3}
Titan (Sand-Air) ****	1.35	188	1.5×10^{-5}

* Taken from Lapotre et al., 2017 [17]. ** Taken from Lapotre et al., 2016 [44] for $\rho_{air} = 0.02$ kg/m³. *** Taken from Lapotre et al., 2016 [44] for $\rho_{air} = 0.002$ kg/m³. **** Taken from Charnay et al., 2015 [48] and from Risbeth et al., 2000 [49].

Typical here are grain sizes of some millimeters. From the figure it can be seen that the ripples in hydraulic models with movable bed can develop lengths of about 0.8 m < L < 1.3 m. Thus, "sand" waves considered as dunes in such models may actually be ripples.

Note that with respect to the results shown in Figures 15–17 in case of wind action, saltation-impact related $v_c^\star$, $\tau_c^\star$ are used (here taken as $0.5\,\tau_{c,drag}^\star$). With drag only, the domain of ripples begins with correspondingly higher values of $v_{c,drag}^\star \approx 1.4 * v_{c,impact}^\star$.
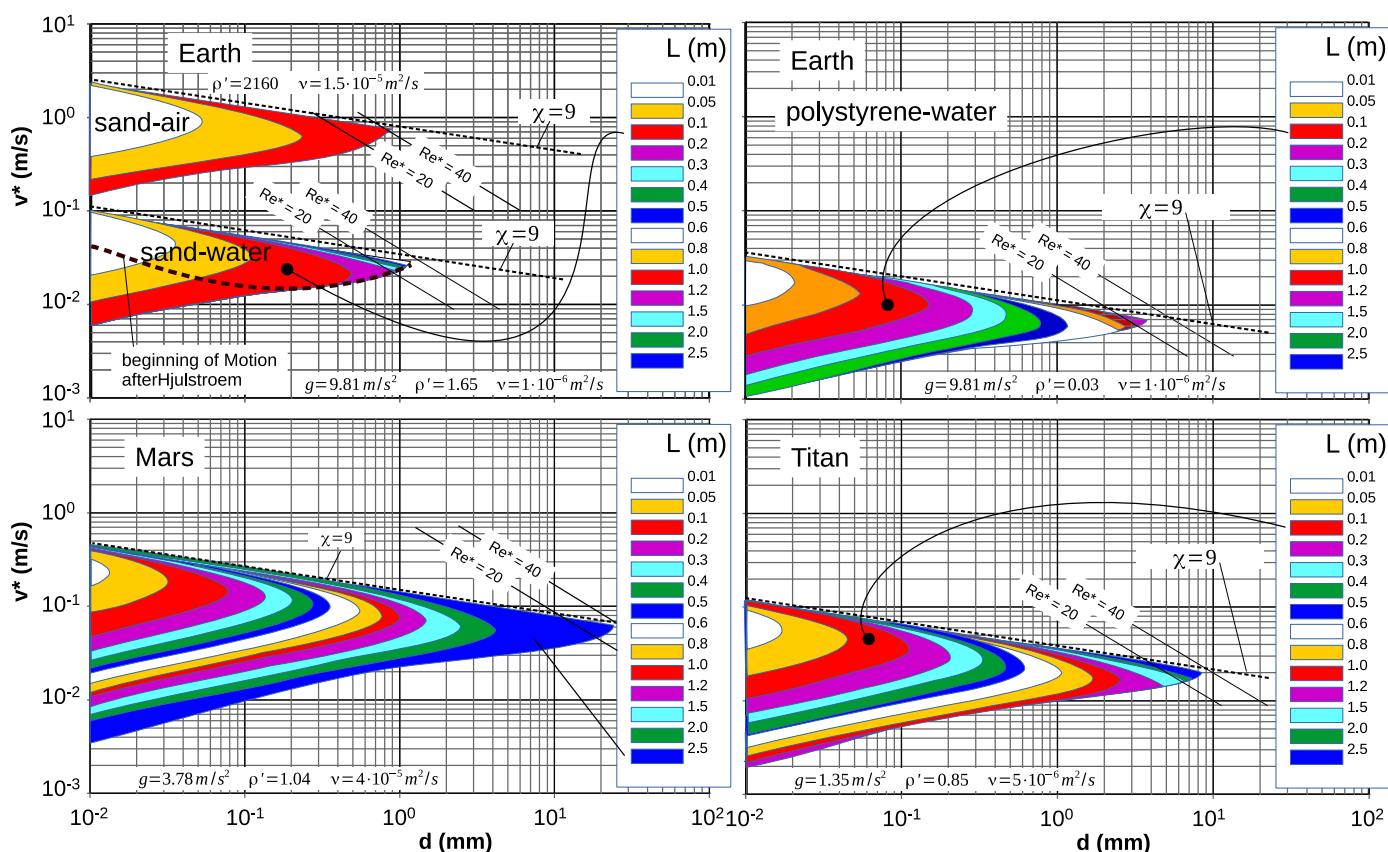
Figure 16. Predicted length of ripples on Earth, Mars, and Titan based on the theory presented here, assuming a completely cohesion-free sediment. Upper row: Earth with sand-water and sand-air (left) and polystyrene-water (right). The dashed curve in the sand-water case shows the effect of sediments with some parts of cohesives on the beginning of motion, analogous to the well-known Hjulström curve. Lower row: Mars (martian sands driven by highly concentrated brines, left) and Titan (ice grains driven by liquid methane flows (right).

In the case of distant planets, the existence and characteristics of ripples indirectly provides information about the fluid flows and winds there. Furthermore, it is important for the approach developed here to show that it also provides plausible results for completely different conditions of viscosity, gravity, and densities.
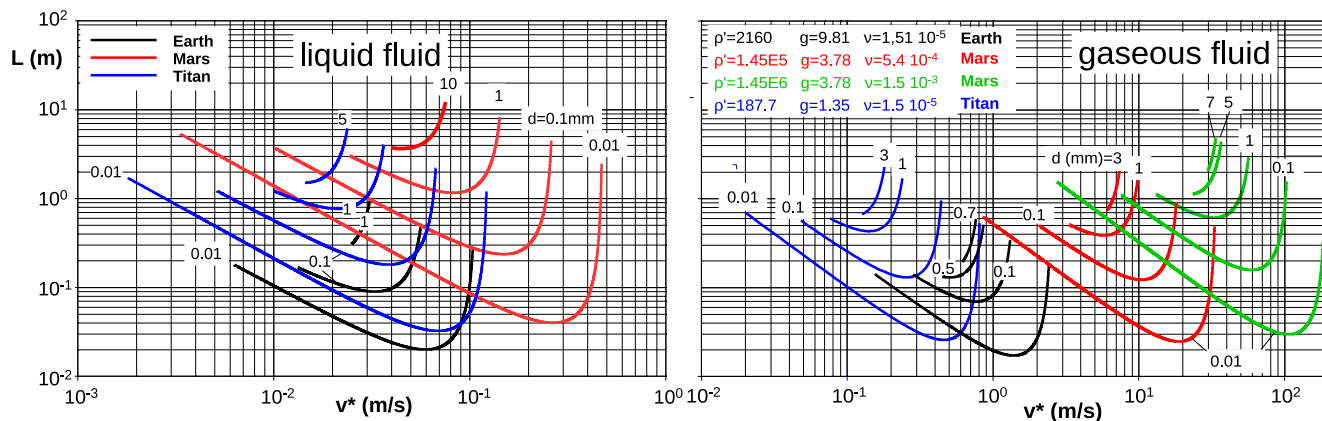
Figure 17. Examples of predicted ripple lengths on Earth, Mars, and Titan based on the theory presented here, noncohesive sediment assumed. (In case of gaseous fluids $\tau_c^\star$ here taken as $\tau_{c,impact}^\star = 0.5\ \tau_{c,drag}^\star$). Right side, red case: Mars air-density data according to Lapotre et al., 2016 [44] assumed with $\rho = 0.02$ kg/m^3, green: $\rho = 0.002$ kg/m^3. Note: Real winds on Mars have been found to reach $v^\star < 4$ m/s.

8. Discussion

To distinguish ripples from dunes, the wavelength of $L \approx 0.6$ m is often used in the literature. In a recent paper, Lapotre et al., 2017 pursue an alternative definition based on data analysis. They use the Yalin parameter χ and empirically define $\chi = 4$ as the ripple limit. According to Lapotre et al., dunes exist at $\chi > 9$ and the range of $4 < \chi < 9$ is defined as a transition.

In the present work, a definition of ripples based on boundary layer theory was developed. For its verification and adjustment, 512 measured data from different authors are available.

The principle of the theory is the fact that an initially viscous boundary layer turns over to turbulence after a certain flow path. This is also the case on the stoss-side of ripples. The turnover causes a significant increase in sediment transport rates, which results in local erosion and thus in a limitation of the ripple length.

The solution of this effect directly describes the ripple lengths in the range of about $0.4 < \chi < 4$. For $\chi < 0.4$, an increasing influence of the suspension potential was found and an associated empirical description is presented. For $\chi > 4$, the acceleration of the flow along the windward slope obviously has an additional influence by pushing out the position of the turnover to turbulence. With reference to the relevant literature, we concluded that ripples can exist up to a dimensionless ripple length of $L^\star \approx 30,000$. With this in mind, we assign the transition region according to Lapotre et al. to ripples According to our results, the domain of ripples is bounded on the one hand by the onset of sediment movement and on the other hand by the dimensionless ripple length $L^\star =< 30,000$. Thereby, with respect to the ripple-dune border, $L^\star = 30,000$ and $\chi = 9$ almost coincide. Another result is that a minimum of ripple lengths occurs at a Yalin number of $\chi \approx 4$.

Exemplary evaluations for ripples on Earth, Mars, and Saturn's moon Titan are presented. In the case of Earth, the developed solution reflects the frequently cited maximum ripple length of about 0.6 m, in both the sand-water and sand-wind cases. The predicted ripples of other planets, some of which are much longer than those on Earth, are also consistent with observations.

In light of the fact that the numerical effects of suspension and acceleration are described empirically, further research is needed with this respect.

9. Conclusions

With the approach presented here, a clear definition of what ripples are can be given. Accordingly, ripples are characterized by a viscous boundary layer along the windward slope and its transition into turbulence. If this is not the case, e.g., because due to the grain size no viscous boundary layer can exist on the windward slope, dunes are formed. Then other mechanisms are effective, which are not the subject of this paper.

Symbols

A	Factor of flow acceleration effect on viscous boundary layer, Equation (33)	-
a_u	critical Reynolds number $v_\infty \lambda / \nu$ für turn from laminar to turbulent boundary layer	-
$a_{u,acc}$	same as a_u but in case of accelerated flow	-
c_f	local drag coefficient	-
d	grain diameter	m
d_m	mean grain diameter $(d_{10} + d_{20} + \ldots d_{90})/9$	m
d_{50}	Grain size, which is exceeded by 50% of its weight	m
D^*	dimensionless grain diameter $= (\rho' g/\nu^2)^{1/3} d = (Re^{*2}/\tau^\star)^{1/3}$	-
g	acceleration of gravity	m/s^2
H	height of bed forms	m
h	mean water depth $= h_1 + H/2$ (Figure 2)	m
h_1	water depth over the crests of ripples and dunes	m
K	key parameter describing the ability to relaminarize a viscous boundary layer, Equation (25)	-
L	length of bed forms	m
$L^\star$	$= v^\star L/\nu$	-
L_s	partial length of bed forms with significant skin friction	m
$Re*$	$= v^\star d/\nu$, particle Reynolds number	-
S	factor describing the effect of suspension on ripple length, Equation (20)	-
v_m	depth and time averaged flow velocity	m/s
v_∞	velocity of the outer flow of the boundary layer	m/s
$v^\star$	shear velocity $= \sqrt{\tau/\rho} = \sqrt{\tau^\star \rho' g d}$	m/s
w	settling velocity	m/s
α	angle of free turbulence	°
β	angle of inclination of the windward slope of ripple and dunes	°
λ_{crit}	critical length after which the boundary layer switches from viscous to turbulent	m
ν	kinematic viscosity of fluid	m^2/s
ρ	density of fluid	kg/m^3
ρ_s	density of sediment	kg/m^3
ρ'	$= (\rho_s - \rho)/\rho$, relative density	-
τ	$= \rho g h I = v^{\star 2} \rho$, shear stress at the bed	N/m^2
$\tau^\star$	$= \tau/((\rho_s - \rho)g d) = v^{\star 2}/(\rho' g d)$, dimensionless shear stress	-
φ	angle of repose = angle of internal friction of sediment	°
χ	Yalin number as defined by Lapotre et al. [17], Equation (5)	-

References

1. Plate, E.J. *Ein Beitrag zur Bestimmung der Windgeschwindigkeitsverteilung in Einer Durch Eine Wand Gestörten Bodennahen Luftschicht [A Contribution to the Determination of the Wind Speed Distribution in a Near-Bed Air Layer Disturbed by a Wall]*; Diss. Techn. Hochschule (TH): Stuttgart, Germany, 1966. (In German)
2. Yalin, M.S. Geometrical Properties of Sand-Waves. *Proc. ASCE* **1964**, *90*, HY5.
3. Allen, J.R.L. *Current Ripples*; North Holland Publishing Company: Amsterdam, The Netherlands, 1968.
4. Kennedy, J.F. The Formation of Sediment Ripples, Dunes and Antidunes. *Annu. Rev. Fluid Mech.* **1969**, *1*, 147–168. [CrossRef]
5. Fredsoe, J. Sediment Ripples and Dunes. *Ann. Rev. Fluid Mech.* **1982**, *14*, 13–37.
6. Ashley, G.M. Classification of large-scale subaquaeous bed forms: A new look on an old problem. *J. Sediment. Petrol.* **1990**, *60*, 160–172.
7. Zanke, U. *Über den Einfluß von Kornmaterial, Strömungen und Wasserständen auf die Transportkörper in Offenen Gerinnen [On the Effect of Bedmaterial, Currents and Water Depth on the Parameters of Ripples and Dunes in Open Channels]*; Mitt. des Franzius-Instituts der TU Hannover: Hannoverm, Germany, 1976; Volume 44. (In German)
8. Southard, J.; Boguchwal, A. Bed configurations in steady unidirectional water flows. Synthesis of flume data. *J. Sediment. Petrol.* **1990**, *60 Pt 2*, 658–679. [CrossRef]
9. Chabert, J.; Chauvin, J.L. Formation des dunes et des rides dans les modèles fluviaux. *Bull. CREC Chatou* **1963**, *4*, 1–51.
10. Bonnefille, R.; Pernecker, L. Le début d'entraînement des sediments sous l'action de la 'houle. *Bull. CREC Chatou* **1966**, *15*.
11. Vollmers, H.; Giese, E. Discussion on "Instability of Flat Bed in Alluvial Channels". *Proc. ASCE* **1970**, doi:10.1061/JYCEAJ.0002820. [CrossRef]
12. Wieprecht, S. *Entstehung und Verhalten von Transportkörpern bei Grobem Sohlenmaterial [Origin and Behavior of Dunes in Coarse Bed Material]*; University of the German Federal Armed Forces: Neubiberg, Germany, 2001; ISBN 3-486-26518-0. (In German)
13. Van den Berg, J.H.; van Gelder, A. A new bedform stability diagram, with emphasis on the transition of ripples to lane flows over fine sand. *Spec. Publ. Int. Ass. Sediment* **1993**, *17*, 11–21.
14. Burr, M.; Perron, J.T.; Lamb, M.P.; Rossman, P.I.; Collins, G.C.; Howard, L.S.; Moore, J.M.; Adamkovics, M.; Baker, V.R.; Drummond, S.A.; et al. Fluvial features on Titan: Insight from morphology and modeling. *Geol. Soc. Am. Bull.* **2013**, *125*, 299–321. [CrossRef]
15. Kleinhans, M.G. *Phase Diagrams of Bed States in Steady, Unsteady, Oscillatory and Mixed Flows*; Geology Utrecht University: Utrecht, The Netherlands, 2005; Corpus ID: 56390344.
16. Yalin, M.S. On the Determination of Ripple Geometry. *ASCE J. Hydraul. Eng.* **1985**, *111*, 1148–1155. [CrossRef]
17. Lapotre, M.G.A.; Lamb, M.P.; McElroy, B. *What Sets the Size of Current Ripples?* The Geological Society of America: Boulder, CO, USA, 2017.
18. Barton, J.R.; Lin, P. *A Study of the Sediment Transport an Alluvial Channels*; Report No. 55, JRB 2; Civil Engineering Department, Colorado A and M College, Agricultural and Mechanical College: Fort Collins, CO, USA, 1955.
19. Vanoni, V.A.; Brooks, N.H. *Laboratory Studies of the Roughness and Suspended Load of Alluvial Streams*; Report No. E-68; Publication No. 149; California Institute of Technology: Pasadena, CA, USA, 1957.
20. Stein, R.A. Laboratory studies of total load and apparent bed load. *J. Geophys. Res.* **1965**, *70*, 1342–1381. [CrossRef]
21. Guy, H.P.; Simons, D.B.; Richardson, E.V. *Summary of Alluvial Channel Data from Flume Experiments, 1956–1961*; Prof. Paper 462-1; U.S. Geological Survey: Washington, DC, USA, 1966.
22. Williams, G.P. *Flume Experiments on the Transport of Coarse Sands*; Sediment Transport in Alluvial Channels. U.S. Geol. Survey Prof. Paper 562-B; U.S. Geological Survey: Washington, DC, USA, 1967.
23. Alexander, L.J.D. On the Geometry of Ripples Generated by Unidirectional Open Channel Flows. Master's Thesis, Queens University, Kingston, ON, Canada, 1980.
24. Bishop, C.T. On the Time-Growth of Dunes. Master's Thesis, Queen's University, Kingston, ON, Canada, 1977.
25. Mantz, P.A. Bedforms produced by fine, cohesionless, granular and flakey sediments under subcritical water flows. *Sedimentology* **1978**, *25*, 83–103. [CrossRef]
26. Grazer, A.J. Experimental Study of Current Ripple Using Medium Silt. Master's Thesis, Cambridge Massachusets Institute of Technology, Cambridge, MA, USA, 1982.
27. Gabel, S.L. Geometry and kinematics of dunes during steady and unsteady flows in the Calamus River, Nebraska, USA. *Sedimentology* **1993**, *40*, 237–269. [CrossRef]
28. Baas, J.H. A flume study on the development and equilibrium morphology of current ripples in very fine sand. *Sedimentology* **1994**, *41*, 185–209. [CrossRef]
29. Venditti, J.G.; Church, M.A. Bed form initiation from a flat sand bed. *J. Geophys. Res.* **2005**, *110*. [CrossRef]
30. Kühlborn, J. Wachstum und Wanderung von Sedimentriffeln [Growth and Migration of Sediment Ripples]. Technische Berichte über Ingenieurhydrologie und Hydraulik. Master's Thesis, Institut für Wasserbau. Techn. Hochschule Darmstadt, Darmstadt, Germany, 1993. (In German)
31. Schlichting, H. *Grenzschicht-Theorie [Boundary Layer Theory]*; Verlag G. Braun: Karlsruhe, Germany, 1965. (In German)
32. Schlichting, H.; Gersten, K. *Grenzschicht-Theorie [Boundary Layer Theory]*; Springer: Berlin/Heidelberg, Germany, 2005; p. 160. (In German)

33. Dey, S.; Paul, P.; Fang, H.; Pahdi, E. Hydrodynamics of flow over two-dimensional dunes. *Phys. Fluids* **2020**, *32*, 025106. [CrossRef]

34. Dey, S.; Paul, P.; Fang, H.; Pahdi, E. Reynolds stress anisotropy in flow over two-dimensional ridgid dunes. *R. Soc. Publ. Proc. Roy. Soc. A* **2020**, *476*, 20200638. [CrossRef]

35. Zhao, C. Free surface flow over two-dimensional dunes under different flow regimes. *IOP Conf. Ser. Earth Environ. Sci.* **2021**, *647*, 012125. [CrossRef]

36. Vanoni, V.A. Experiments on the Transportation of Suspended Sediment by Water. Master's Thesis, California Institute of Technology, Pasadena, CA, USA, 1940.

37. Toorman, E.A.; Bruens, A.W.; Kranenburg, C.; Winterwerp, J.C. Fine Sediment Dynamics in the Marine Environment. In *Proceedings in Marine Science*, 5th ed.; Elsevier: Amsterdam, The Netherlands, 2002; Volume XV, 713p, ISBN 0-444-51136-9.

38. Zanke, U. *Berechnung der Sinkgeschwindigkeiten von Sedimenten [Determination of Settling Velocities of Sediments]*; Mitt. des Franzius-Instituts der Univ. Hannover: Hannover, Germany, 1977; Volume 46. (In German)

39. McNown, J.S.; Malaika, J. Effects of particle shape on settling velocity at low Reynolds numbers. *Trans. Am. Geophys. Union* **1950**, *31*, 511–522. [CrossRef]

40. Launder, B.E. *Laminarization of the Turbulent Boundary Layer by Acceleration*; Volume Rep. No. 77; MIT Gas Turbine Laboratory, Massachusetts Institute of Technology: Cambridge, MA, USA, 1964.

41. Pschernig, M. Messung der Relaminarisierung der Druckseitigen Grenzschicht einer Turbinenschaufel Mittels Heißfilmanemometrie [Measurement of the Relaminarization of the Pressure-Side Boundary Layer of a Turbine Blade by Means of Hot Film Anemometry]. Master's Thesis, Institut für Thermische Turbomaschinen und Maschinendynamik, TU Graz, Graz, Austria, 2017. (In German)

42. Duran, O.F.; Andreotti, B.; Claudin, P.; Winter, C. A unified model of ripples and dunes in water and planetary environments. *Nat. Geosci.* **2019**, *12*, 345–350. [CrossRef]

43. Almeida, M.; Parteli, E.; Andrade, J.S.; Herrmann, H.J. Giant saltation on Mars. *Proc. Natl. Acad. Sci. USA* **2008**, *105*, 6222–6226. [CrossRef] [PubMed]

44. Lapotre, M.G.A.; Ewing, R.C.; Lamb, M.P.; Fischer, W.W.; Grotzinger, J.P.; Rubin, D.M.; Lewis, K.W.; Ballard, M.J.; Day, M.; Gupta, S.; et al. Supplementary Materials for: Large wind ripples on Mars: A record of atmospheric evolution. *Science* **2016**, *54*, 353. [CrossRef]

45. Shields, A. *Anwendung der Ähnlichkeitsmechanik und der Turbulenzforschung auf die Geschiebebewegung*; Mitt. der Preussischen Versuchsanstalt für Wasser-, Erd- und Schiffbau: Berlin, Germany, 1936; Volume 26.

46. Hjulström, F. *Studies of the Morphological Activity of Rivers as illustrated by the River Fyris*; Bulletin of the Geological Institution of the University of Upsala: Upsala, Sweden, 1935; pp. 221–527.

47. Perron, J.T.; Lamb, M.P.; Koven, C.D.; Fung, I.Y.; Yager, E.; Adamkovics, M. Valley formation and methane precipitation rates on Titan. *J. Geophys. Res. Planets* **2006**, *111*. [CrossRef]

48. Charnay, B.; Barth, E.; Rafkin, S.; Narteau, C.; Lebonnois, S.; Rodriguez, S.; Courrech du Pont, S.; Lucas, A. Methane storms as a driver of Titan's dune orientation. *arXiv* **2015**, arXiv:1504.03404.

49. Risbeth, H.; Yelle, R.V.; Mendillo, M. Dynamics of Titan's thermosphere. *Planet. Space Sci.* **2000**, *48*, 51–58. [CrossRef]